

Predicting plasticity in disordered solids from structural indicators

D. Richard,^{1,2} M. Ozawa,^{3,4} S. Patinet,⁵ E. Stanifer,² B. Shang,^{6,7} S.A. Ridout,⁸ B. Xu,^{6,9}
G. Zhang,⁸ P.K. Morse,¹⁰ J.-L. Barrat,⁷ L. Berthier,^{4,11} M.L. Falk,^{12,9,13,14} P. Guan,⁶
A.J. Liu,⁸ K. Martens,⁷ S. Sastry,¹⁵ D. Vandembroucq,⁵ E. Lerner,¹ and M.L. Manning²

¹*Institute for Theoretical Physics, University of Amsterdam, Science Park 904, Amsterdam, Netherlands*

²*Department of Physics, Syracuse University, Syracuse, NY 13244*

³*Laboratoire de Physique de l'Ecole Normale Supérieure, ENS, Université PSL,
CNRS, Sorbonne Université, Université de Paris, F-75005 Paris*

⁴*Laboratoire Charles Coulomb, UMR 5221 CNRS-Université de Montpellier, Montpellier, France*

⁵*PMMH, CNRS UMR 7636, ESPCI Paris, PSL University,
Sorbonne Université, Université de Paris, F-75005 Paris, France*

⁶*Beijing Computational Science Research Center, Beijing 100193, China*

⁷*Univ. Grenoble Alpes, CNRS, LIPhy, 38000 Grenoble, France*

⁸*Department of Physics and Astronomy, University of Pennsylvania, Philadelphia, PA 19104*

⁹*Mechanical Engineering, Johns Hopkins University, Baltimore, Maryland 21218, USA*

¹⁰*Department of Chemistry, Duke University, Durham, North Carolina 27708, USA*

¹¹*Department of Chemistry, University of Cambridge,
Lensfield Road, Cambridge CB 2 1EW, United Kingdom*

¹²*Materials Science and Engineering, Johns Hopkins University, Baltimore, Maryland 21218, USA*

¹³*Physics and Astronomy, Johns Hopkins University, Baltimore, Maryland 21218, USA*

¹⁴*Hopkins Extreme Materials Institute, Johns Hopkins University, Baltimore, Maryland 21218, USA*

¹⁵*Jawaharlal Nehru Center for Advanced Scientific Research, Jakkur Campus, Bengaluru 560064, India*

Amorphous solids lack long-range order. Therefore identifying structural defects — akin to dislocations in crystalline solids — that carry plastic flow in these systems remains a daunting challenge. By comparing many different structural indicators in computational models of glasses, under a variety of conditions we carefully assess which of these indicators are able to robustly identify the structural defects responsible for plastic flow in amorphous solids. We further demonstrate that the density of defects changes as a function of material preparation and strain in a manner that is highly correlated with the macroscopic material response. Our work represents an important step towards predicting how and when an amorphous solid will fail from its microscopic structure.

How can we predict when and where a material will fail? For disordered solids, including many food and cosmetic products, screens and cases for smartphones, and even mud and gravel perched on a hillside, this fundamental question remains a challenge. Under small deformations or forces, such amorphous materials respond as an elastic solid, but beyond a critical threshold the materials yield and exhibit extensive irreversible plastic deformation.

At the moment, we cannot easily predict from first-principles whether a given material will fail abruptly and catastrophically, termed brittle failure, or flow slowly and steadily, known as ductile flow. Moreover, we can not predict when or where it will fail, and we lack global design principles for how we might change the microscopic structure of these materials in order to control failure mechanisms.

One reason disordered solids are so challenging to understand is that, unlike crystals, their microscopic structure lacks long-range order. In crystals it is easy to identify a defect where the crystalline order is broken, and unsurprisingly plasticity is initiated at certain types of these defects. Over the past 50 years, analogous structural defects have been proposed in amorphous solids [1], but it has proven more difficult to identify these and connect them to deformation and failure.

For this reason, theoretical work has largely remained

disconnected from simulations. Several fairly successful theories have posited that there is no correlation of particle rearrangements with the inherent microstructure [2], while others such as Shear Transformation Zone (STZ) [3, 4], Soft Glassy Rheology (SGR) [5] and elastoplastic models [6] assume the existence of structural defects, without specifying the precise definition of these defects. Perhaps more problematically, all these theories are phenomenological in the sense that they contain fitting parameters that we do not know how to extract from first principles, i.e. from the microstructure and interactions between the constituent particles of the material.

Fairly recently, large-scale computer simulations of glass-formers have reinvigorated the search for structural defects. Examples of promising approaches include mapping the local shear modulus [7], highlighting regions that are excited by linear and nonlinear vibrational modes [8–12], or quantifying the structure in more complex ways e.g. using machine learning [13, 14]. A particularly literal and successful approach applies strain to small regions within a simulation to determine which are closest to yielding [15, 16].

Until now there have been three main drawbacks to this line of inquiry. First, there has never been a consistent methodology for evaluating whether a given indicator that identifies structural defects works well for predicting deformation and failure, although efforts to

wards this goal have been made [15]. Second, it has not been clear whether a given method works best only on a particular model system or the interaction potential for which it was designed, or whether some methods work well universally across different disordered solids. Finally, computer-generated amorphous solids have historically been vastly more ductile than those in real experiments, and so it was difficult to simulate brittle materials that exhibit catastrophic failure. Recent methodological developments [17, 18] now allow very deep supercooling of model polydisperse liquids, to temperatures comparable to and even lower than what can be achieved with laboratory liquids. These liquids, when quenched to zero temperature, form ultra-stable glasses that exhibit brittle failure [19].

In this article we employ these computational tools to conduct a comprehensive and quantitative comparative study of how well several recently-proposed structural indicators predict plastic activity in two-dimensional model glasses formed using a wide range of preparation conditions. We develop a standard methodology for comparing these indicators to one another, and to the complex deformation fields that result from the applied deformation.

We find that different classes of structural indicators are not always strongly correlated, suggesting that different paradigms for identifying structural defects are sensitive to distinct structural information. With a few exceptions, the indicators we investigated are excellent at predicting deformation in ductile and brittle materials over short strain scales (0.1% in the system sizes studied), and several remain correlated beyond 10% strain, highlighting that structure really does govern plastic deformation in these zero-temperature materials under simple shear. The quality of a given indicator does not vary much between the two interaction potentials we studied. In contrast, their predictive capabilities do change with glass stability: indicators are generally less accurate in ductile glasses, where many regions are soft even at zero strain. An exception to this rule occurs in the ultra-stable glasses accessible via swap Monte Carlo – in these materials many of the structural indicator fields change so much before the first plastic rearrangement that the indicator field at zero strain is not highly predictive. Importantly, we demonstrate that free volume (or any measure of a local density), historically used to predict plasticity in metallic glasses, performs much worse than other indicators. Finally, we are able to follow the complete strain history of a given brittle sample and we find that our indicators are able to capture an anisotropic spatial distribution of soft regions before shear banding.

We shear systems of 2D soft disks using a standard athermal quasi-static (AQS) protocol, where the only control parameters are the imposed strain γ and the strain increment $\delta\gamma$ [20]. Fig. 1(a-b) shows that the mechanical response quantified by plots of the shear stress σ versus γ , where different curves correspond to different material preparation protocols. Fig. 1(a) corresponds to a standard glass former, a bidisperse packing

of particles with a Lennard-Jones (LJ) interaction potential; glasses were formed by cooling equilibrium states by means of conventional molecular dynamics methods [21]. Fig. 1(b) corresponds to polydisperse (POLY) disks [17] interacting via purely repulsive interactions; liquid states spanning a wide range of supercooling temperatures were equilibrated using the swap Monte Carlo method, and quenched to the glassy phase with a minimization algorithm. Plastic instabilities associated with deformation and particle rearrangements correspond to instantaneous drops in the stress. Qualitatively, we see that some material preparation protocols generate less-stable, ductile solids where small plastic instabilities occur frequently until the system approaches a steady state. Other preparation protocols generate ultra-stable brittle solids which behave nearly elastically until they fail catastrophically around 6 or 7% strain ($\gamma_{\text{yielding}} \simeq 0.07$). In order to compare these two very different material systems, we study the average strain at the first instability, $\langle\gamma_{\text{min}}\rangle$ (Fig. 1(c)), which is a good indicator for material stability/ductility for a given finite N , and correlates strongly with other previously developed measures for stability (Supplementary Fig. S1). Another indicator, the magni-

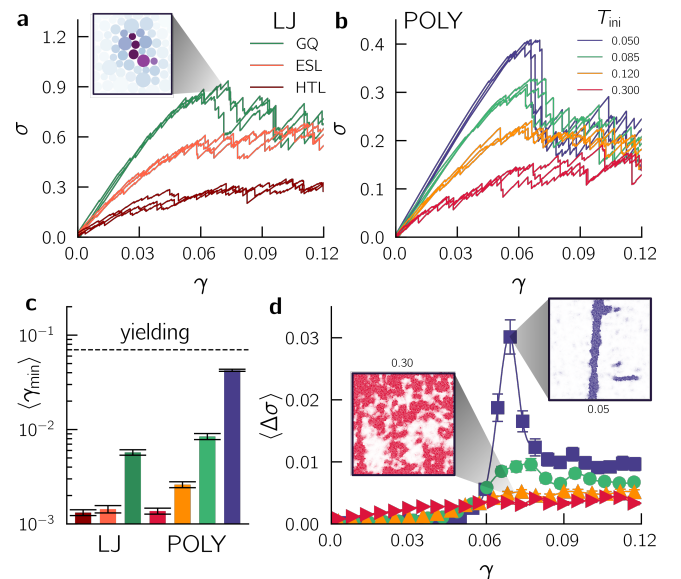


FIG. 1: **Probing plasticity from ductile to brittle glasses.** (a) Typical stress-strain curves for the LJ system prepared via three different quench protocols. Inset shows a typical plastic event where dark particles indicate non-affine rearrangements. (b) Typical stress-strain curves for the POLY system quenched from 4 initial temperatures T_{ini} . (c) Average strain at the first plastic instability ($\langle\gamma_{\text{min}}\rangle$) for the different systems and protocols (with $N = 10^4$ particles). The dashed line indicates the yield strain $\gamma_{\text{yielding}} \simeq 7\%$. (d) Average stress drop $\langle\Delta\sigma\rangle$ as a function of the strain γ for the POLY system. Snapshots show the cumulative non-affine displacements observed after yielding in a very stable glass (top right) and a typical ductile glass quenched instantaneously from a high temperature liquid (bottom left). Errorbars are sample to sample fluctuations.

tude of the average stress drop $\langle \Delta\sigma \rangle$, is an order parameter for the macroscopic yielding transition [19], exhibiting a sharp peak at the macroscopic yielding transition in brittle systems (Fig. 1(d)) associated with the formation of a system-spanning shear band (right inset).

Having characterized the macroscopic material properties of these systems, we next study how plastic deformation correlates with proposed indicators for structural defects. Although many different correlation functions have been proposed in previous work, here we adopt a very simple cumulative rank correlation [15], in order to fairly compare structural indicators with vastly different magnitudes and distributions, and to avoid setting an arbitrary threshold (details provided in SI). From this methodology, we define $C = C(\gamma_{str}, \gamma_{pl})$ as the correlation between a snapshot of the structure at strain γ_{str} and the plastic deformation field at a strain γ_{pl} .

In the following, we distinguish five different families of structural indicators: (i) eight purely structural ones that only require the position of particles and not their interaction potential (red in Fig. 2), (ii) one machine learning-based method that is also structural but require a training on a subset of shear deformations (purple), (iii) three based on the linear response/harmonic vibrational modes with no information about the applied strain (green), (iv) four that quantify the linear response to a specialized applied strain, which here is simple shear (blue), (v) three going beyond the non-linear response (orange). Details are in the SI. The full spearman indicator to indicator correlation C_s (defined in the SI) is shown in Fig. 2(a) for the gradually quenched binary Lennard-Jones system. The majority of purely structural indicators correlate strongly with each other but are not strongly correlated with indicators based on the linear response. This suggests that the two classes of indicators are capturing different features, likely because the latter has explicit access to the forces across bonds, which encode longer-range elastic interactions across the contact network.

Previous work has demonstrated that initialization protocol has a substantial impact where and how a glassy material fails under shear. Therefore, we first study how the structural indicators evaluated at zero strain, $\gamma = 0$, correlate with the plastic deformation that occurs at the first plastic event, at a strain $\gamma_{pl}(1)$. Fig. 2(b,c) show the cumulative rank correlation $C_{min} = C(0, \gamma_{pl}(1))$ for all the indicators studied in the most ductile (HTL) and least ductile (GQ) LJ glasses. Note that C_{min} is evaluated at vastly different strains in different systems, at approximately $\gamma \sim 0.1\%$ in ductile glasses, and approximately $\gamma \sim 5\%$ in the most brittle glasses. We observe a qualitative agreement between the two different protocols with some quantitative change in the prediction as the sample becomes more stable. Indicators constructed from normal modes (from \mathcal{M} to φ_γ) perform extremely well, with a correlation C_{min} approaching unity. These indicators can even perform as well as the residual plastic strength $\Delta\tau_y$, which is a highly nonlinear method that

locally shears a small portion of the material centered around a particle i and measures how much additional stress is needed to induce yielding. This result confirms many observations that loci of plasticity are directly connected to the presence of low-frequency excitations that control the response of a system upon external driving [9, 11].

The majority of structural based indicators perform badly, with two important exceptions: the steric bond order Θ and the machine learning-based softness field S , which are highly correlated with each other and with soft modes as shown by C_s in Fig. 2(a), highlighted by a yellow box. The indicator Θ highlights particles that strongly depart from sterically favored configurations with little particle overlap, and thus is a local measure of frustration. The fact that Θ is so similar to the agnostic machine learning method suggests that the machine algorithm has learned to identify such frustration, too. In metallic glasses, plastic rearrangements do correlate strongly with unfavored local structures [22]. This connects to recent evidence that internal stresses caused by frustrations during the quench are responsible for quasi-localized excitations [23] and strongly echoes with experimental work on metallic glasses [24].

In Fig. 2(d), we summarize our results by plotting C_{min} for the three different quench protocols shown in Fig. 1(a) and ordering them according to the degree of stability of the sample. For visibility, we only display one of the best structural indicators in each family (Θ , S , \mathcal{M} , $\text{naf}\mu$, and $\Delta\tau_y$). The predictive power increases as the system becomes less ductile, consistent with Ref. [21]. In the least ductile LJ systems, structural indicators based on vibrational modes or frustrated geometric configurations work very well to predict the next plastic event. This is especially impressive since less ductile materials must be strained further before triggering the next plastic event.

Fig. 2(e) shows the correlation C_{min} for the same structural quantities as in Fig. 2(d), now for a polydisperse system prepared using swap Monte Carlo (POLY). Again, the initialization protocols are ranked from most ductile to most brittle, which is controlled by the equilibrium parent temperature T_{ini} from which the system is minimized. Recalling from Fig. 1(c) that the first three types of POLY systems have ductility and stability very similar to the three types of LJ systems, we notice that Fig. 2(d) and (e) are quite similar if we restrict ourselves to those data points. This is also highlighted by the similarities in C_{min} across nearly all structural indicators between ductile LJ (Fig. 2(c)) and POLY (Fig. 2(f)) systems. Taken together, these results suggest that the attractive interaction and degree of polydispersity related to the interaction potential have only a small influence on the predictive power of a given indicator.

In contrast, the stability/ductility of the material very strongly influences the predictive power – for almost all of the conditions studied, the predictive power increases with decreasing ductility. This can be rationalized by realizing that the system dynamics are noisy, and so when

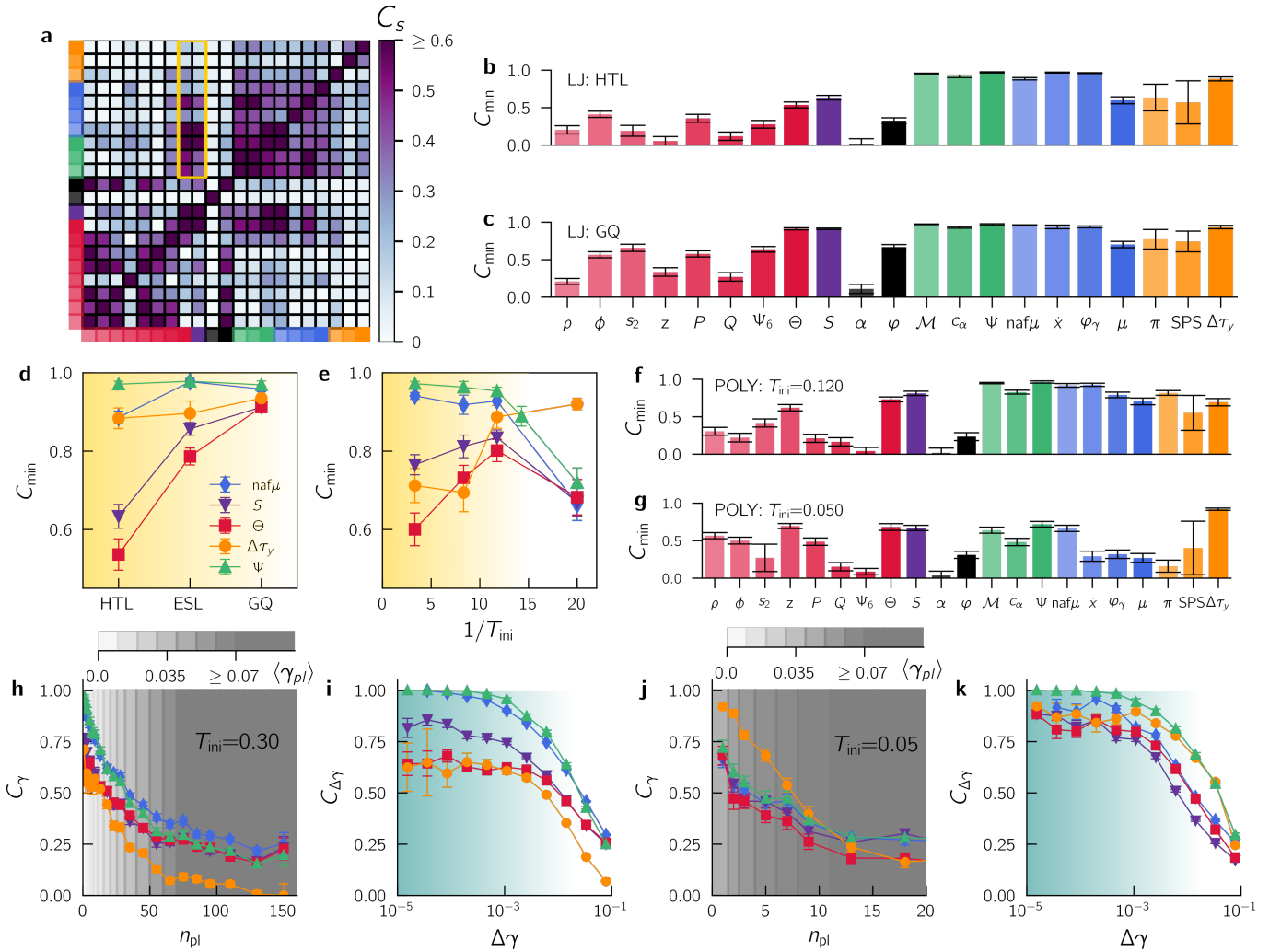


FIG. 2: Comparison of structural indicators. Local density ρ , free volume ϕ , excess entropy s_2 , contact force number z , voronoi anisotropy P , divergence of the voronoi anisotropy Q , hexatic bond orientational order Ψ_6 , steric bond order Θ , softness field S , local thermal expansion α , potential energy φ , low-frequency vibrational modes \mathcal{M} , local heat capacity c_α , vibrality ψ , atomic non-affine shear modulus $\text{naf}\mu$, non-affine velocity \dot{x} , change of potential energy upon deformation φ_γ , local shear modulus μ , non-linear vibrational modes π , Saddle Point Sampling SPS, residual plastic strength $\Delta\tau_y$. (a) Indicator to indicator Spearman cross correlation C_s for the less ductile (GQ) LJ glasses. (b-c) and (f-g) Correlation $C_{\min} = C(0, \gamma_{pl}(1))$ between a structural field computed at $\gamma = 0$ and the first plastic event. Binary LJ data are shown for the most (HTL) to the least (GQ) ductile glasses in (b) and (c), respectively. (d) shows the same information as in (d) but plotted as a function of the inverse of the parent temperature. Polydisperse glasses data prepared by SWAP are shown for mildly ($T_{\text{ini}} = 0.12$) and very stable glasses ($T_{\text{ini}} = 0.05$) in (f) and (g), respectively. (e) shows the same information as in (d) but plotted as a function of the inverse of the parent temperature. (h,j) Correlation decay $C_\gamma = C(0, \gamma_{pl}(n_{pl}))$ between a structural field computed at $\gamma = 0$ and the n th plastic event in a system composed of 10^4 particles. The underlying gray gradient indicates the corresponding average plastic strain $\langle \gamma_{pl} \rangle$ ranging linearly from $\gamma = 0$ (transparent) to $\gamma \geq \gamma_{\text{yielding}}$ (opaque). (i,k) Correlation growth $C_{\Delta\gamma} = C(\gamma_{pl} - \Delta\gamma, \gamma_{pl})$ between a structural field $\Delta\gamma$ away from a plastic event located at γ_{pl} . Results are for ductile glasses (h-i) and brittle glasses (j-k) prepared at $T_{\text{min}} = 0.30$ and $T_{\text{min}} = 0.05$, respectively. The different colors and symbols corresponds to the same structural indicators as shown in (d) and (e).

a large fraction of the system is relatively soft it is more difficult to predict which of those soft regions will fail first.

On the other hand, the most brittle systems we study – Fig. 2(g) and the right-most points in Fig. 2(e) – buck this trend. These correspond to ultra-stable glasses that can only be formed using swap Monte Carlo. In those

systems, the predictive power of vibrational modes, softness, and Θ are all lower. We also observe the same drop in Saddle Point Sampling (SPS), which highlights that the relevant saddles in the potential energy landscape are not present at $\gamma = 0$ and form during the elastic branch. A direct consequence is the reversibility of first inelastic events in very stable glasses (confirmed in

SI). In contrast, the prediction offered by the residual plastic strength keeps increasing. This suggests that in very stable glasses, linear response is insufficient to predict plasticity and that one needs access to non-linear response.

One possible explanation for this observation is that the first plastic event is nearly an order of magnitude further away in strain for the most brittle materials compared to the other material preparations (Fig. 1(c)). To test this hypothesis, we study how the correlation between structure and deformation changes with the number of plastic events that have occurred since the state was prepared at $\gamma = 0$. For the ductile glass, we see that the correlation function decays smoothly as the system approaches the yielding regime, identified by the grey shading (Fig. 2(h)). The correlation for some structural indicators remains above the noise floor even beyond 50 plastic events or 10 % strain, consistent with previous studies [9, 15]. In brittle glasses, with the exception of $\Delta\tau_y$, there is instead a strong decrease in correlation after just a handful of plastic events (Fig. 2(j)). This suggests that significant changes to the indicators are occurring along *elastic branches* in the absence of any plasticity, and that the longer length of these elastic branches is indeed the reason why, for most indicators, predictive capabilities are low in the most brittle glasses. It also explains why $\Delta\tau_y$ is far superior in this case – because $\Delta\tau_y$ is measured only after the system yields, it has access to these transformed states far along an elastic branch.

While some of the indicators are computationally expensive and therefore can only be computed at $\gamma = 0$, it is possible to compute other indicators along the strain trajectory. For these indicators, we also explore how well they capture deformation as a function of the strain until the next plastic event, $\Delta\gamma$, averaged over all plastic events. These data are shown with $C_{\Delta\gamma} = C(\gamma_{pl} - \Delta\gamma, \gamma_{pl})$ in Fig. 2(i) for a ductile glass, and (k) for a brittle glass. In both systems, the correlation for the best indicators is nearly unity until a differential strain of 10^{-3} , which is close to the average distance between plastic events for a system of this size. Beyond this strain scale, the predictive power decreases exponentially, suggesting that the system gradually loses memory of its past state over a characteristic strain scale of 10^{-1} .

Many phenomenological models that predict plastic deformation and failure rely on largely untested assumptions about the characteristics of structural defects, such as their strain distance to threshold or density. Now we are finally in a position to begin to test some of those assumptions, by quantifying properties of our calculated structural fields and studying how different structural indicators contribute different insights into macroscopic material response. In particular, we can utilize a structural indicator to isolate regions likely to rearrange and follow their spatial evolution during deformation. Here, we propose to follow various sheared states along the stress-strain curve of a brittle glass (Fig. 3(a)).

We first focus on the initial state ($\gamma = 0$). We ex-

tract an estimate for the strain distance to the next instability as $\Delta\tau_y/\tilde{\mu}$, with $\tilde{\mu}$ being the bulk shear modulus. In Fig. 3(b), we plot the distribution $P(\Delta\tau_y/\tilde{\mu})$ at zero strain, for our most ductile ($T_{\min} = 0.3$ (red)) and most brittle ($T_{\min} = 0.05$ (blue)) computationally modeled glasses. In both cases, we find a power-law tail at low $\Delta\tau_y/\tilde{\mu}$, highlighting the presence of anomalously soft regions. However, the density of regions close to a plastic rearrangement changes drastically between the ductile and brittle material (about 2 orders of magnitude), which is illustrated by the left-most snapshots where particles that are less than 3% in strain from threshold are colored in white. We observe the same decrease in the number of low-energy excitations (extracted by localizing modes lying below the onset frequency of the power law tail in the density of states, see SI) and indicated by black crosses, consistent with other studies [25, 26]. We find that the purely structural indicator Θ , which does not require information about the interaction between particles, is also able to resolve a decrease in the number of particles belonging to highly disordered motifs ($\Theta > 0.1$), demonstrated quantitatively in the distribution $P(\Theta)$ in Fig. 3(c) and qualitatively in the left-most bottom snapshots. Since the tail of $P(\Theta)$ changes by only one order of magnitude instead of two, it incorrectly labels some regions as soft even when the distance to threshold ($\tau_y/\tilde{\mu}$) is high. Nevertheless, these data demonstrate that some purely structural methods easily accessible to experimentalists can effectively be used to sort samples with respect to their ductility. While Θ works well for these simulations with spherically symmetric interaction potentials, similar trends are seen in also in the structural softness metric S , as shown in Fig. S10 and S11, which can be applied to a wide range of simulations and experimental systems [27].

One consequence of the change seen in $P(\Delta\tau_y/\tilde{\mu})$ for brittle glasses is that the system can be deformed up to 5% of strain with only a minor plastic activity. This leads us to state point (2) in Fig. 3(a). Here localized excitations have softened, which translates into a shift of $P(\Delta\tau_y/\tilde{\mu})$ towards $\Delta\tau_y/\tilde{\mu} \rightarrow 0$. In other words, soft regions present in the tail seen in Fig. 3(b), move closer to their critical threshold, in agreement with elasto-plastic models where $\Delta\tau_y$ is assumed to decrease by $\tilde{\mu}\gamma$. Hence, we observe a homogeneous distribution of regions that are about to yield, similar to those seen in ductile glasses. Purely structural indicators are less sensitive to this softening.

The situation is somewhat different at the onset of shear band formation, after a series of small rearrangement events. Looking at (3), we first observe that (i) more regions are about to yield and (ii) the spatial distribution is more anisotropic compared to (2). Comparing Θ between (2) and (3), we observe an increase of regions with a high local disorder. The region where the shear band is going to form appears to be softer than the rest of the system, which is confirmed more quantitatively in the SI and in agreement with recent work [28]. Finally, the

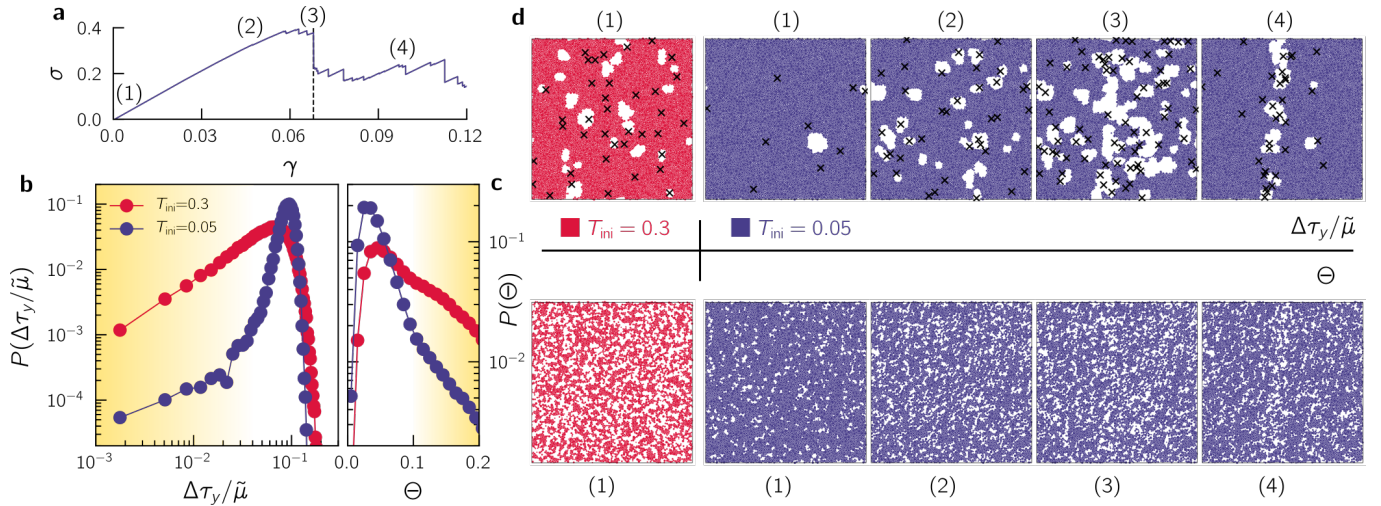


FIG. 3: **Yielding pathway.** (a) Stress-strain curve of a brittle glass (the same sample as shown in Fig. 1(d)). (b) Probability distribution function of the (strain) distance to threshold $\Delta\tau_y/\bar{\mu}$ at zero strain for ductile (red) and brittle (blue) glasses. (c) Probability distribution of the measure of microscopic disorder Θ . (d) Snapshots highlight the spatial distribution of soft regions (white color) with particles having $\Delta\tau_y/\bar{\mu} < 3\%$ and $\Theta > 0.1$, respectively. Black crosses show the location of low-energy excitations. Similar trends occur for the structural softness indicator, Fig S11.

system yields and reaches a transient shear-banded state (4). We observe that the majority of our structural indicators are able to locate the shear band. In particular, we observe an array of low energy excitations perfectly aligned with regions close to their threshold. Moreover, Θ reveals that the microstructure inside the band is highly disordered, reinforcing the link between local disorder, low-energy excitations, and residual plastic strength.

Taken together, these results demonstrate that shear-driven rearrangements in amorphous solids are deeply encoded in the structure. In ductile systems, many of the structural indicators that have been previously proposed are highly predictive of deformation at yielding and beyond. Our work indicates that two purely structural indicators (machine learning and Θ), which do not require any knowledge of the interaction potential and can be immediately applied to experimental systems, perform comparably to more complicated methods in ductile solids. Another surprising observation is that the linear modes, which can be extracted from time-averaging of two-particle correlation functions in experiments [29], outperform all other methods in ductile materials.

This work represents an important step towards quantifying how a disordered configuration of grains in a sandpile or molecules in a glass encode localized excitations that evolve and interact to generate large-scale flow and failure, and sets the stage for rationally designing or engineering materials with prescribed macroscopic flow prop-

erties.

Acknowledgments

M. Ozawa thanks Hua Tong from the University of Tokyo for fruitful discussions and help with implementation. We are grateful for the support of the Simons Foundation for the Cracking the Glass Problem Collaboration Awards No. 348126 to Sid Nagel (D. Richard), No. 454945 (S. Ridout, A. J. Liu), No. 454947 (P. Morse and M. L. Manning), No. 454933 (M. Ozawa and L. Berthier). S. Patinet acknowledges the support of French National Research Agency through the JCJC project PAMPAS under grant ANR-17-CE30-0019-01. M.L. Falk acknowledges support from the US National Science Foundation under Grant No. DMR-1910066/1909733. We acknowledge support from Simons Investigator Award No. 327939 (A. J. Liu), the University of Pennsylvania MRSEC NSF-DMR-1720530 (G. Zhang), and NSF-DMR-1352184 (E. Stanifer). B. Xu., B. Shang and P. Guan acknowledge the funding support from the NSF of China (Grants No.U1930402) and the computational support from the Beijing Computational Science Research Center(CSRC). S. Sastry acknowledges support through the J C Bose Fellowship, DST, India. E. Lerner was supported by the Netherlands Organisation for Scientific Research (Vidi Grant 680-47-554/3259).

- [1] F. Spaepen, *Acta metallurgica* **25**, 407 (1977).
 [2] F. Ritort and P. Sollich, *Advances in physics* **52**, 219 (2003).

- [3] A. Argon, *Acta metallurgica* **27**, 47 (1979).
 [4] M. L. Falk and J. S. Langer, *Physical Review E* **57**, 7192 (1998).

- [5] P. Sollich, F. Lequeux, P. Hébraud, and M. E. Cates, *Physical review letters* **78**, 2020 (1997).
- [6] A. Nicolas, E. E. Ferrero, K. Martens, and J.-L. Barrat, *Reviews of Modern Physics* **90**, 045006 (2018).
- [7] M. Tsamados, A. Tanguy, C. Goldenberg, and J.-L. Barrat, *Physical Review E* **80**, 026112 (2009).
- [8] A. Widmer-Cooper, H. Perry, P. Harrowell, and D. R. Reichman, *Nature Physics* **4**, 711 (2008).
- [9] M. L. Manning and A. J. Liu, *Physical Review Letters* **107**, 108302 (2011).
- [10] L. Gartner and E. Lerner, *Physical Review E* **93**, 011001 (2016).
- [11] J. Zylberg, E. Lerner, Y. Bar-Sinai, and E. Bouchbinder, *Proceedings of the National Academy of Sciences* **114**, 7289 (2017).
- [12] H. Tong and H. Tanaka, *Physical Review X* **8**, 011041 (2018).
- [13] E. D. Cubuk, S. S. Schoenholz, J. M. Rieser, B. D. Malone, J. Rottler, D. J. Durian, E. Kaxiras, and A. J. Liu, *Physical review letters* **114**, 108001 (2015).
- [14] S. S. Schoenholz, E. D. Cubuk, D. M. Sussman, E. Kaxiras, and A. J. Liu, *Nature Physics* **12**, 469 (2016).
- [15] S. Patinet, D. Vandembroucq, and M. L. Falk, *Physical review letters* **117**, 045501 (2016).
- [16] S. Patinet, A. Barbot, M. Lerbinger, D. Vandembroucq, and A. Lemaître, *arXiv preprint arXiv:1906.09818* (2019).
- [17] L. Berthier, D. Coslovich, A. Ninarello, and M. Ozawa, *Physical review letters* **116**, 238002 (2016).
- [18] A. Ninarello, L. Berthier, and D. Coslovich, *Phys. Rev. X* **7**, 021039 (2017).
- [19] M. Ozawa, L. Berthier, G. Biroli, A. Rosso, and G. Tarjus, *Proceedings of the National Academy of Sciences* p. 201806156 (2018).
- [20] C. E. Maloney and A. Lemaître, *Physical Review E* **74**, 016118 (2006).
- [21] A. Barbot, M. Lerbinger, A. Hernandez-Garcia, R. García-García, M. L. Falk, D. Vandembroucq, and S. Patinet, *Physical Review E* **97**, 033001 (2018).
- [22] J. Ding, S. Patinet, M. L. Falk, Y. Cheng, and E. Ma, *Proceedings of the National Academy of Sciences* **111**, 14052 (2014).
- [23] E. Lerner and E. Bouchbinder, *Physical Review E* **97**, 032140 (2018).
- [24] Y. Zhang, W. Wang, and A. Greer, *Nature materials* **5**, 857 (2006).
- [25] E. Lerner and E. Bouchbinder, *Physical Review E* **96**, 020104 (2017).
- [26] L. Wang, A. Ninarello, P. Guan, L. Berthier, G. Szamel, and E. Flenner, *Nature communications* **10**, 26 (2019).
- [27] E. D. Cubuk, R. Ivancic, S. S. Schoenholz, D. Strickland, A. Basu, Z. Davidson, J. Fontaine, J. L. Hor, Y.-R. Huang, Y. Jiang, et al., *Science* **358**, 1033 (2017).
- [28] A. Barbot, M. Lerbinger, A. Lemaître, D. Vandembroucq, and S. Patinet, *Physical Review E* **101**, 033001 (2020).
- [29] K. Chen, W. G. Ellenbroek, Z. Zhang, D. T. Chen, P. J. Yunker, S. Henkes, C. Brito, O. Dauchot, W. Van Saarloos, A. J. Liu, et al., *Physical review letters* **105**, 025501 (2010).